PROCEEDINGS OF THE INTERNATIONAL CONFERENCE
NANOMATERIALS: APPLICATIONS AND PROPERTIES
Vol. **3** No 2, 02NNSA08(7pp) (2014)

Dielectric Relaxation in $Sr(Co_{1/3}Nb_{2/3})O_3$ Compound – A Candidate For Microwave Applications

Bhagwanti S. Bishnoi[1], P.K. Mehta[2,*], C.J. Panchal[3,†], M.S. Desai[3], V.H. Kher[4], D.V. Velykodnyi[5], I.Yu. Protsenko[5,‡]

[1] *Krishna Institute of Engineering and Technology, Department of Applied Sciences, Ghaziabad- 201 206 (U.P), India*
[2] *Department of physics, Faculty of Science, The M. S. University of Baroda, Vadodara-390002 Gujarat, India*
[3] *Applied Physics Department, Faculty of Technology & Engineering, The M. S. University of Baroda, Vadodara-390001 Gujarat, India*
[4] *Applied Physics Department, Polytechnic, The M. S. University of Baroda, Vadodara, 390002 Gujarat, India*
[5] *Sumy State University, 2, R.-Korsakov Str., 40007 Sumy, Ukraine*

(Received 11 July 2014; published online 29 August 2014)

Relaxor ferroelectric compounds $Sr(B_{1/3}Nb_{2/3})O_3$, where ($B = Mg^{2+}$, Co^{2+}, Cu^{2+}), synthesized by standard solid state reaction technique, exhibit strong correlation between structure, dielectric and transport behavior. The structure changes from highly distorted monoclinic structure in Mg^{2+} and Co^{2+} substituted samples to partially distorted Tetragonal structure in Cu substituted samples. In Cu^{2+} based system significant Jahn-Teller distortion induced enhancements in dielectric properties have also been observed. Further, weak Jahn-Teller distortion due to unevenly occupied t_{2g} levels in Co^{2+} produces intermediate rise in ε' as well as inbuilt flexibility to conduction electron movement enhances dielectric loss (tan δ). On the other hand, strong Jahn-Teller effects in Cu^{2+} substituted compound, due to unevenly occupied e_g levels, results in large enhancement in ε' and frequency exponent 's' (> 500 at 300 K temperature & at 10 KHz frequency). The UV-Vis studies give the wide energy band gap semi conducting values {$E_g \geq 3.00$ eV}. The improved physical properties of $Sr(Cu_{1/3}Nb_{2/3})O_3$ compound makes it suitable for energy storage devices as well as microwave device applications at wide frequency range.

Keywords: Oxides, X-ray diffraction, Impedance studies, Dielectric properties, Optical properties.

PACS numbers: 81.20.Ka, 81.05.Je, 61.05.cf

1. INTRODUCTION

During the last few decades many classes of electronic oxide ceramic are dominated by ABO_3 perovskites and perovskite-related compounds. The unique range of responses, coupled with the flexibility of perovskites in accommodating a broad spectrum of atomic substitutions at A and B- sites, provides a robust platform for probing correlations between structure, bulk chemistry, and properties. Alterations in the B-site order can induce ferroelectric-to-relaxor transitions in Pb-based systems or order-of-magnitude changes in the dielectric loss properties of alkaline earth-based microwave dielectrics [1-3]. In recent years $A(B'_{1/3}B''_{2/3})O_3$ type perovskites have attracted much attention as a candidate for the microwave dielectric materials due to its defect induced relaxor behavior with high dielectric constant and low dielectric loss tangent at room temperature[4]. Lots of materials like $Sr(Mg_{0.33}Nb_{0.67})O_3$,[SMN] [5-8], $(Sr(Fe_{0.5}Nb_{0.5})O_3$, [SFN] [9, 10], $Sr(Zn_{0.33}Nb_{0.67})O_3$,[SZN] [11, 12], $Sr(Yb_{0.5}Nb_{0.5})O_3$ [13], $Sr(Cu_{0.33}Nb_{0.67})O_3$[SCuN] [14-19], $Sr(Co_{0.33}Nb_{0.67})O_3$ [SCoN] [19-22] have been investigated and various physical properties like Detailed crystal structure analysis with Retiveld Refinement, dielectric properties, photo catalyst properties, doping at A site in SCuN to reduce *Tc* Conductivity studies, etc have been studied by above researchers. The complex impedance spectroscopy consists of measuring the real and imaginary part (Z' and Z'') of impedance of dielectric sample at various temperatures and for different frequencies.

In the present work we have investigated the Crystal structure, Microstructure, Cole-Cole analysis, Dielectric properties, Optical Studies and Conductivity studies of all the samples in the series, i.e.[SCuN], [SMN] and [SCoN], by means of the x-ray diffraction, SEM and impedance spectroscopy. The dielectric constant is found out to be very high and its transition temperature is reduced in SCoN compound compared to SMN and SCuN [19].

2. EXPERIMENTAL DETAILS

2.1 Sample Preparation

The $Sr(B_{1/3}Nb_{2/3})O_3$, where ($B = Mg^{2+}$, Co^{2+}, Cu^{2+}), ceramic is prepared using a two stage synthesis process. In the first stage, $(B_{0.33}Nb_{0.67})O_3$ precursor phase was produced from MgO, CuO or Co_3O_4(≥ 99 %), Nb_2O_5(≥ 99 %) powders taken in stoichiometric proportions. The powders were mixed homogenously and pressed lightly into pellets and calcined at 900 °C for 6 hrs. After the initial precursor heating cycles, a stoi-

* pkmehta_phy@yahoo.co.in
† cjpanchal_msu@yahoo.com
‡ protsenko@aph.sumdu.edu.ua

chiometric amount of $SrCO_3$ is added, intimately mixed, and calcined at 900 °C overnight to decompose the carbonate. Prior to each heating cycle, the sample was grounded and palletized using a uniaxial press. Multiple heating cycles, with intermediate grindings and repelletizing were performed in the temperature range of 900 °C to a final temperature of 1200 °C. In each cycle the sintering was carried out in air for 12 hrs with the pallet of size 12 mm in diameter and 1.4 mm in thickness.

2.2 X-ray Diffraction

X-ray diffraction (XRD) measurements were carried out on powdered samples using a high resolutions Shizmadu X-ray diffractometer 6000 employing $CuK_{\alpha 1}$ radiations at 40 KV and 30 mA ($\lambda = 1.5402$ Å). The diffraction patterns were recorded from 10° to 110° at a step of 0.02°.

2.3 Scanning Electron Microscopy

For micro structural analysis the cylindrical pellets were coated with 50 Å Aluminum layer in order to avoid the electron charge on the surface, as samples are highly insulating. The microstructures of the samples were studied by Scanning Electron Microscopy (JEOL JSM 5600).

2.4 UV-Vis Spectroscopy

The UV / VIS Spectroscopy was measured by Perkin Elmer Precisely Lambda 950 instrument. Its range was from 300-1500 nm. All the measurement was carried out in Absorbance mode at room temperature.

2.5 Dielectric Measurement

The temperature-dependent dielectric measurements were carried out using an LCR meter (1260 Solartron) in the frequency range of 50-3.2E7 Hz. The SCoN ceramic sample (of thickness 1.40 mm and diameter 12 mm) were polished with silver paste and heat treated at 200 °C in order to remove micro-cracks (if any). Polished discs were placed between two electrode connected to LCR meter and operated in the temperature range room temp to 350 °C. These results were found to be reproducible.

3. RESULTS AND DISCUSSIONS

3.1 XRD Analysis

XRD pattern of $Sr(Co_{0.33}Nb_{0.67})O_3$ [SCoN], at room temperature is shown in Fig. 1. All the reflection peaks of the x-ray profile have been indexed using least-square method with the help of standard indexing program Powder-X. The diffraction analysis confirms that compound is single phase with monoclinic structure at room temperature with $\beta = 95.45°$ ($a = 5.79909$ Å, $b = 8.57682$ Å, $c = 13.45582$ Å). Overall volume of the unit cell is 669 Å [3].

On comparing lattice parameters of SCoN with reported values of $Sr(Mg_{0.33}Nb_{0.67})O_3$ [SMN][5] we observed that the substitution of atom with lower ionic radii (Mg^{2+} by Co^{2+}) reduces the lattice parameters and volume. The structure changes from highly distorted monoclinic structure in Mg^{2+} and Co^{2+} substituted samples to partially distorted Tetragonal structure in Cu substituted samples.

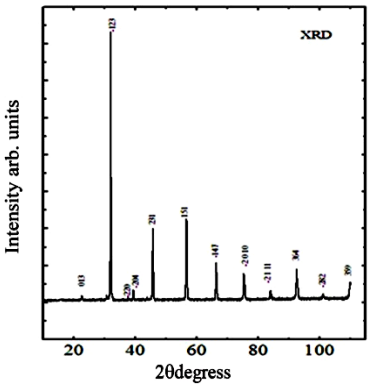

Fig. 1 – X-ray diffraction pattern of SCoN

3.2 Scanning Electron Microscopy

The micro structural investigations shown in Fig. 2 reveal conglomerated structures with noticeable porosity in SCoN samples. The conglomeration is probably due to trapping of moisture during crystallization producing semi liquid phase at grain boundaries.

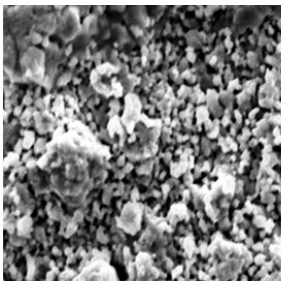

Fig. 2 – SEM image of SCoN

The crystal structure and microstructure reveals that there would be drastic modifications in dielectric / ferroelectric behavior of SCoN compounds.

3.3 Frequency Dependence of Impedance

The variation of real part of impedance (Z') with

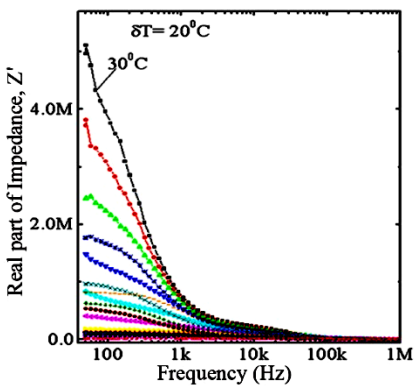

Fig. 3 – Real part of Impedance (Z') vs. frequency at different temperatures

frequency at various temperatures is shown in Fig. 3. The magnitude of Z' was found to decrease with increase in temperatures. The trend of impedance versus frequency plot provides an indication of increasing conduction with temperature and frequency.

The presence of space charge polarization is predicted on the basis of observed high value of Z' at lower frequency and temperature in the sample [23-24]. In addition at higher frequency (> 100 KHz) the value of Z' was found to merge together for all temperatures, i.e. becoming temperature and frequency independent, suggesting a possible release of space charge now [24, 25].

The variation of imaginary part of impedance (Z'') with frequency at different temperature is shown in Fig. 4. The appearance of temperature dependent peaks (Z''_{max}) at a characteristics frequency ($\omega_{max} = 2\pi f_{max}$) can be related to the type and strength of the electrical relaxation phenomena in the system. This behaviour shows the presence of space charge in the system [24, 25]. The shift in the position of peak with temperature shows a temperature dependent relaxation process, possibly a modified non-debye type relaxation in the system. We observed dispersion of the resultant curves in lower frequency region at different temperatures also visible in other systems [24, 25]. It appears in Fig. 4 that the peak positions in the pattern (Z'' versus T) appear to be shifting towards higher temperature side with increase in frequency.

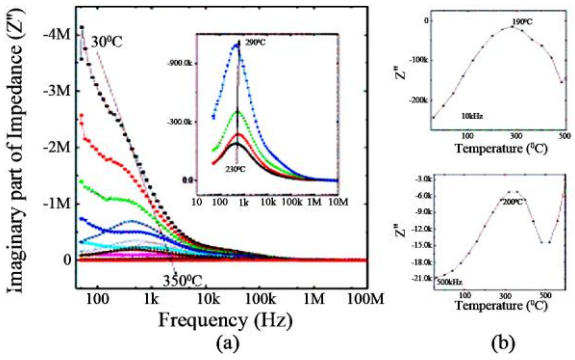

(a) Imaginary part of Impedance, Z'' versus Frequency.
(b) Imaginary part of Impedance, Z'' versus Temperature.

Fig. 4 – Imaginary part of Impedance (Z'') vs. frequency at different temperatures. Inset (b) shows Z'' vs. frequency from 230 °C-290 °C

This evidence clearly indicates temperature dependent electrical relaxation phenomena in the material. It has also been observed that from room temperature to 190 °C there is substantial increase in f_{max} values towards higher frequency side while after 200 °C the f_{max} values start decreasing and again increases after 300°. This effect may be due to merging of grain and grain boundary impedance into single arc (Cole-Cole) at 200 °C. This can be linked to possible effect of intermediate temperature on the microstructure and electrical properties of the material. At a later stage it can be seen that similar effect is also been observed in the dielectric constant ((ε') versus T) plot in Fig. 10. There is a sharp transition at 190 °C in ε' versus T. Further, all the curves found to merge at a specific frequency in the higher frequency region. This is interpreted as due to the reduction in space charge polarization at higher frequency [24, 26, 27]. In perovksites system the major mode of charge transport is a multiple hopping process [28]. Hopping process normally takes place across the potential barriers set up by the lattice structure and local environment of other atoms / ions.

The relaxation time involved can be calculated using the relation

$$2\pi f_{max}\,\tau = 1, \qquad (1)$$

where, f_{max} is frequency at the Z'' maxima.

The τ value is different till 190 °C and after that it shows a cycle of decrease and increase. Clear peak formation is observed only from 110 °C. Therefore we have considered the data from 110 °C to 350 °C. The activation energy is obtained in the region of 110 °C to 190 °C.

3.3.1 Cole-Cole Analysis

The impedance data at room temperature do not take the shape of a semi circle in the Cole-Cole plot rather it presents a straight line with large slope suggesting the insulating behaviour. The slope of the line was found to decrease with increasing temperature and at 100 °C and beyond, a clear semicircle can be traced out. The presence of single semicircle shows the presence of grain interior (bulk) property of the material. However, as the temperature increases the presence of second semicircular arc appears and it is found that at 200 °C, as shown in the Fig. 5, the Cole-Cole forms again a single semicircular arc.

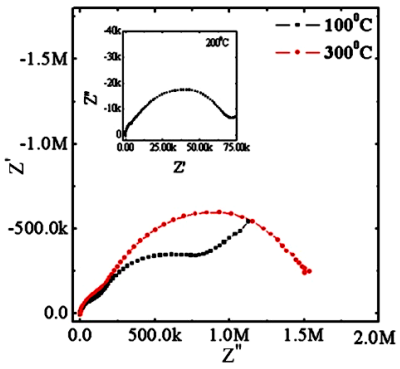

Fig. 5 – Cole-Cole plots of SCoN at two different temperatures. Inset shows the cole-cole for temp 200 °C

It means there is some change in the mechanism of conduction in the material accompanied by a phase transition. The SCoN material undergoes a possible transition from ferroelectric to paraelectric phase. This is clearly visible in the Z'' vs Freq plot in the form of fluctuations in f_{max} values after 200 °C. The semicircle pattern in the Cole-Cole plots can be expressed as an equivalent electrical circuit consisting of a parallel combination or resistive and capacitive element [29]. Fig. 5 shows the complex impedance spectrum of SCoN at different temperatures (100, 300 °C) and the inset shows the Cole-Cole of 200 °C with single semicircular arc. The high frequency dispersion curves are

attributed to the bulk properties of the material and they are consistently been correlated [30] to be due to the parallel combination of the bulk resistance (R_b) and bulk capacitance (C_b) of the sample (SCoN). The low frequency second dispersion curve has been assigned to the grain boundary conduction. The experimental data is fitted with an equivalent circuit consisting of a parallel combination of resistance and capacitance. The Cole-Cole plot for two different temperatures is shown in Fig. 5. The value of bulk resistance (R_b) and grain boundary resistance (R_{gb}) has been obtained from the intercept of the semicircular arc on real axis (Z') [30]. Further, it appears from Fig. 5 and Table 1 that grain boundary resistance decreases with rise in temperature. Similar effects were also been reported in other compounds [30]. It indicates that the grain boundary effect have assisted in lowering the barrier to the motion of charge carriers paving the way for increased electrical transport with rise in temperature. The obtained value the relaxation time was calculated using the relation $\tau = Rc$ and found to decrease with increasing temperature.

In addition, it has been reported in literature that electrical properties and impedance behavior of a ceramic oxide is a phase sensitive parameter. The appearance of grain boundary effects (second semicircular arc in the impedance spectrum) is sometimes related to be arising due to segregation / phase separation in a mixed phase system as well as due to local ordering changes at the grain boundary [31-35]. We have observed the variation of grain boundary resistance and grain boundary conductivity as a function of temperature and are shown in Fig. 6 and 7.

Table 1 – Variations of electrical parameters (bulk and grain boundary) as a function of temperature

Temp(^{0}C)	R_s	R_b(ohm)	C_b(F)	dc resistivity (ohm-m)	σ	R_{gb}(ohm)	C_{gb}(F)	σ
30	2100	250000	3.97E-11	2.101E7	9.925E-6	3.78E6	1.85E-10	6.44E-4
50	2100	230000	4.97E-11	1.933E7	1.143E-5	2.68E6	2.50E-10	6.7 E-4
70	1900	210000	5.97E-11	1.765E7	1.253E-5	1.76E6	2.90 E-10	5.10 E-4
90	1900	154590	6.97E-11	1.299E7	1.077E-5	816300	4.11 E-10	3.35 E-4
110	1890	109960	7.97E-11	9.241E6	8.763E-6	406300	4.91 E-10	1.99 E-4
130	1870	49900	8.37E-11	4.194E6	4.176E-6	126300	3.91 E-10	4.938E-5
150	1200	19900	9.17E-11	1.672E6	1.824E-6	59300	3.11 E-10	1.84 E-5
170	400	9900	9.97E-11	832077	9.870E-7	31300	3.00 E-10	9.39E-6
190	400	5900	1.01E-10	495844	5.954E-7	21300	2.98 E-10	6.34 E-6
200	109.4	5530				19980	1.01 E-10	2.01 E-6

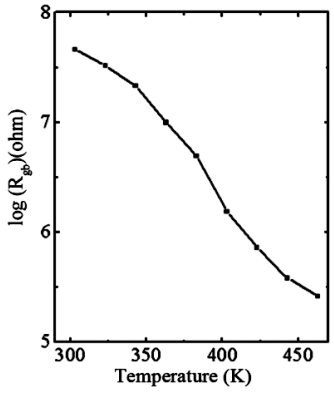

Fig. 6 – Variation of grain boundary resistance (R_{gb}) as a function of temperature

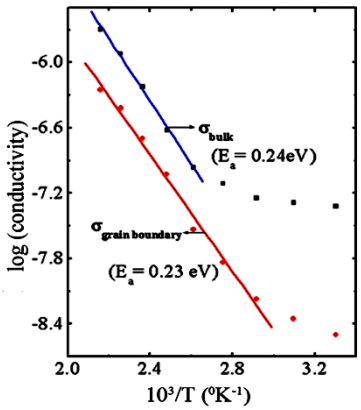

Fig. 7 – Variation of frequency independent conductivity due to grain (bulk) and grain boundary effects as a function of temperature

The variation of grain boundary resistance as a function of temperature (Fig. 6) shows a monotonic decrease in the grain boundary resistance (R_{gb}) with rise in temperature indicating a predominant role of grain boundary in governing the electrical behavior of the system at higher temperatures. This effect was also observed by Pradhan et al. [30] in $NaNdTiO_4$ and been suggested to play a crucial role in determining the nature of electrical conduction in the material. We have also attempted to separately evaluate the grain (bulk) and grain boundary conductivity as a function of temperature from impedance spectrum.

The plots are shown in Fig. 7. The activation of SCoN has been estimated and it is 0.23 eV for grain boundary and 0.24 eV for grain (bulk).

This suggests that the conducting species responsible for both the bulk and grain boundary effects are the same. Further, both of these effects are simultaneously getting affected around 200 °C due to possible change in type of conduction.

3.4 Frequency Dependence of Dielectric Properties

The frequency dependence of dielectric constant (ε')

and dielectric loss tangent (tan δ) is shown in Fig. 8 and 9. The dielectric constant is calculated using the relation

$$\varepsilon' = Cp / C_0, \qquad (2)$$

$C_0 = \varepsilon_0 A / d$ is the capacitance of the empty cell ($\varepsilon_0 = 8{,}85 \cdot 10^{-12}$ F m^{-1}, A is the cross-sectional area of the flat surface of the pellet and d is its thickness).The frequency dependence of the dielectric permittivity and the dielectric loss of SCoN ceramic for various temperatures are plotted in Fig. 8 and 9.

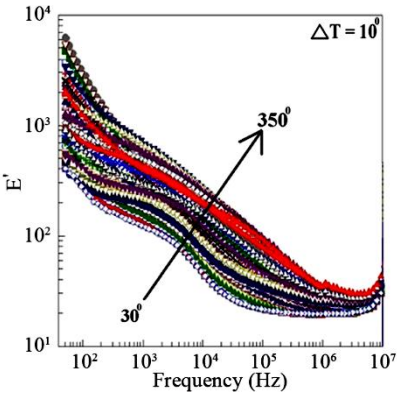

Fig. 8 – Angular frequency dependence of the real part of dielectric constant (ε') with frequency at different temperatures

At room temperature, the real part of dielectric permittivity (ε') has a value of 252 at 100 Hz, and it gradually decreases as frequency increases. Further, ε' values in low frequency region (below 1 kHz) increases significantly as a function of temperature. This behavior is consistent with the other common ferroelectrics [36].

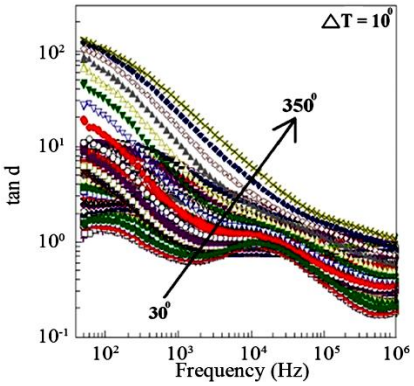

Fig. 9 – Angular frequency dependence of dielectric loss tangent (tan δ) with frequency at different temperatures

U. Intatha et al. [36] and references therein suggested that such a higher values of ε' at lower frequencies are likely to be due to the presence of different types of polarizations (i.e., interfacial, dipolar, atomic, ionic, electronic contribution) in the material. But at high frequencies, however, some of the above-mentioned polarizations may have less contribution in ε'. The high value of ε' in the low frequency region is explained using Maxwell-Wagner (MW) polarization effect or interfacial polarization. Thus high values of permittivity are not usually intrinsic, but rather associated with heterogeneous conduction in the grain and grain boundary of the compounds [36]. It is noted that here grains of the sample are separated by more insulating inter grain barriers therefore generating a boundary layer capacitor [37]. Further, an increase in temperature leads to increase in ε' in the low frequency range, but became ineffective at higher frequencies. Here the dielectric loss (tan δ) was observed to be very high and it decreases with increasing temperature and frequency.

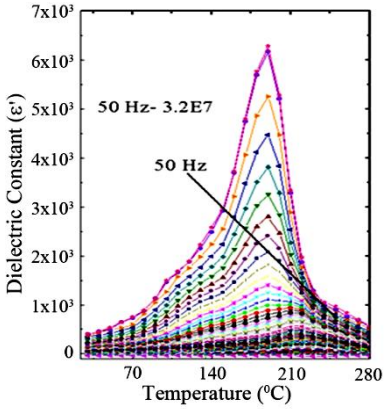

Fig. 10 – Temperature dependence of the real (ε') part of the Electrical Permittivity

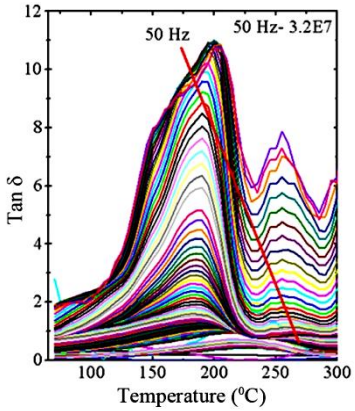

Fig. 11 – Temperature dependence of dielectric loss tangent (tan δ)

The temperature dependence of dielectric constant and loss parameter as a function of frequency is shown in Fig. 10 and 11. The data are taken from 50 Hz-3.2 E7 Hz. We observed the transition temperature of SCoN to be at ~ 190 °C and the value of dielectric constant is 6293 at 50 Hz. Further increase in frequency and temperature, the peak start shifting towards higher temperature which is a typical relaxor phenomenon.

The system shows different relaxation process which is also observed in impedance plots Fig. 4. The results match well with the impedance plots. Again the observed dielectric loss is found to be higher at lower frequencies, which is likely to be due to space charge polarization effect in the system.

Probably the higher conductivity observed in Cobalt substituted samples is due to the higher contribution

from the conducting electrons compared to Mg in $Sr(Mg_{0.33}Nb_{0.67})O_3$,[SMN]. But in comparison to SCuN compound [17-19], we found SCoN has lower transition temperature. In Cu^{2+} based system significant Jahn-Teller distortion induced enhancements in dielectric properties have also been observed. Further, weak Jahn- Teller distortion due to unevenly occupied t_{2g} levels in Co^{2+} produces intermediate rise in ε' as well as inbuilt flexibility to conduction electron movement enhances dielectric loss (tan δ). On the other hand, strong Jahn-Teller effects in Cu^{2+} substituted compound, due to unevenly occupied e_g levels, results in large enhancement in ε'. At the same time, $Sr(Cu_{0.33}Nb_{0.67})O_3$[SCuN] [19] sample shows significant fall in dielectric loss (< 0.5) even at elevated temperatures (< 450 K) due to the localization of conduction electrons within oxygen octahedron.

3.5 Frequency Dependence of Electric Modulus

The electric modulus formalism is expressed as

$$Z^*(\omega) = Z' - jZ'' \tag{3}$$

$$M^*(\omega) = M'(\omega) + jM''(\omega) = j\omega CoZ^*(\omega) \tag{4}$$

From Equation (3) and Equation (4) one can get the following Equations (5) and (6)

$$M' = \omega CoZ'' \tag{5}$$

$$M'' = \omega CoZ' \tag{6}$$

Here Co is the vacuum capacitance and given $\varepsilon_0 A / t$, where t is the thickness and A is the area of the sample, ω is the angular frequency and equal to $\omega = 2\pi f$ is the frequency of the applied filed. This formalism is appropriate for exploring electric phenomena due to electrode polarization and bulk phenomena due to conductivity relaxation time [38, 39]. Fig. 12 and Fig. 13 shows the real and imaginary part of electric modulus calculated using Equations (5) and (6).

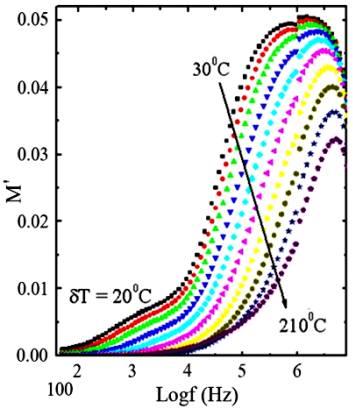

Fig. 12 – The variation of real part of electrical modulus with frequency at various temperatures

The conductivity behavior in the frequency domain is more conveniently interpreted in terms of conductivity relaxation time, τ_o, using electrical modulus (M^*) representation. The M^* representation is now widely used to analyze conductivities by associating a conductivity relaxation time with the process. From Fig. 12, it is obvious that at lower frequen-cies M' values are very small, tend to zero indicating the removal of electrode polarization [38-39], while the increase of M' with increasing frequency and reaching a maximum value M_∞ at high frequency, may be due to the distribution of relaxation processes over a range of frequencies [40]. The observed dispersion in mainly due to conductivity relaxation spreading over a range of frequencies and indicates the presence of a relaxation time, which should be accompanied by a loss peak in the imaginary part of electric modulus versus frequency. The absence of peak in M' is due to the fact that M' in complex electric modulus (M^*) is equivalent to ε' in complex permittivity (ε^*) i.e., M' here represents the ability of the materials to store the energy. The reduction in the values of M' with the increase in temperature indicate the increase in the mobility of the charge carriers.

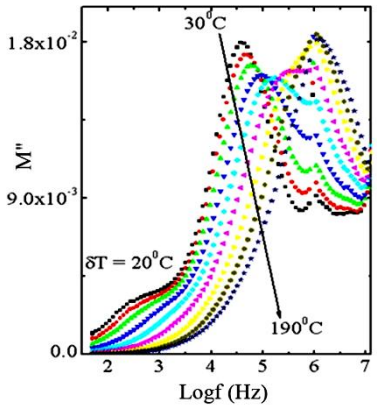

Fig. 13 – The variation of imaginary part of electrical modulus with frequency at various temperatures

Fig. 13 shows the formation of loss peak. It is obvious that M'' exhibiting lower value at lower frequencies might be due to the large value of capacitance associated with the electrode polarization effect [41] resulting from the accumulation of a large amount of charge carriers at the electrode interface. The broad and asymmetric peaks on both sides of the maxima predict the modified Debye type behavior. The region on the left of the peak determines the range in which charge carriers are mobile over long distances, while region to the right is where carriers are confirmed to potential wells being mobile over short distance [39].

3.6 UV- Vis Spectroscopy

Fig. 14 shows optical absorbance spectra of $Sr(Co_{0.33}Nb_{0.67})O_3$ [SCoN] powder on basis of Tau's theory [42]. The optical band gap of SCoN is calculated using Tau'c expression as given in the following equation:

$$\alpha(\hbar\omega) = A(\hbar\omega - E_g)^n \tag{7}$$

where A is a constant related to the effective masses of charge carriers associated with valence and conduction bands, E_g is the optical band gap energy, $E = h\nu$ the photon energy, and $n = 1/2$ or 2, depending on whether the transition is direct or indirect, respectively.

The intersection of the slope of $(\alpha hv)^2$ vs hv curve on the *x*-axis provides band gap energy of the sample α is an absorption coefficient that is calculated by using $\alpha = 2.303 / d \log 10\ 1 / T$, where T is the transmittance and d is the thickness of the sample.

The indirect band gap value is around 3.09 eV. This suggests that system is moving towards wide band semiconducting region from Insulating region due to more free charge carriers.

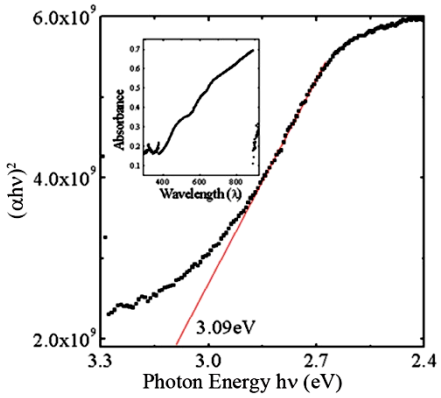

Fig. 14 – Tau plot of UV-visible absorption data for the calculation of band gap energy of SCoN. (Inset shows Absorbance versus Wavelength of SCoN)

4. CONCLUSION

The samples of Sr($Co_{0.33}Nb_{0.67}$)O_3 [SCoN] have been prepared in single Monoclinic phase with morphological features exhibiting agglomerated grain formations. The frequency dependence of real and imaginary part of impedance analysis shows modified non-debye type of relaxation mechanism. The nature of Cole Cole plot reveals the distinct contribution of grain (bulk) and grain boundary to the electrical behaviour, but merge into single contribution around 200 °C. This can be correlated to micro-structural phase changes around 200 °C in the semi-liquid phase of SCoN. The frequency dependence of dielectric constant shows dispersion with colossal ε' values. The losses are found to be high due to Co induced electron doping in SCoN compound. The UV-Vis studies reveal that its band gap is in the wide band gap semiconductor region. The improved dielectric constant in Sr($Co_{0.33}Nb_{0.67}$)O_3 [SCoN] and in particular Sr($Cu_{1/3}Nb_{2/3}$)O_3 compound makes it suitable for energy storage devices as well as microwave device applications at high frequency range.

ACKNOWLEDGMENTS

One of the authors Dr. Bhagwanti Bishnoi is very much thankful to the Inter University Accelerator centre (IUAC) New Delhi for providing financial support under the project UFUP-41315 and for providing irradiation and measurement facility. We are also thankful to UGC DRS program for funding experimental facilities in the department.

REFERENCES

1. P.K. Davies, H. Wu, A.Y. Borisevich, I.E. Molodetsky, L. Farber, *Annu. Rev. Mater. Res.* **38**, 369 (2008).
2. L.E. Cross, **151**, 305 (1994).
3. S. Kawashima, M. Nishida, I. Ueda, H. Ouchi, *J. Am. Ceram. Soc.* **66**, 421 (1983).
4. Xifa Long, Ye Zuo Guang, *Appl. Phys. Let.* **90**, 112905 (2007).
5. C.S. Park, H.J. Paik, Nahm S.J.H. Lee, H.M. Park, K.Y. Kim, *J. Mater. Sci. Lett.* **18** 691, (1999).
6. Alo Dutta Chandrahas Bharti, T.P. Sinha, *Physica B* **403**, 3389 (2008).
7. Hwack Joo Lee, Hyun Min Park, Yang Koo Cho, Yong Won Song, Sahn Nahm, Jae-Dong Byun, *J. Am. Ceram. Soc.* **84**, 3032 (2001).
8. Ki Hyun Yoon, Bum Jun Jung, Eung Soo Kim, *J. Mat. Sci. Lett.* **8**, 819 (1989).
9. Y.Y. Liu, X.M. Chen, X.Q. Liu, L. Li, *Appl. Phys. Lett.* **90**, 192905 (2007).
10. Sonali Saha, T.P. Sinha, *J. Appl. Phys.* **99**, 014109 (2006).
11. Makoto Onoda, Jun Kuwata, Kumiko Kaneta, Keiichiro Toyama, Shoichiro Nomura, *Jpn. J. Appl. Phys.* **21**, 1707 (1982).
12. M. Thirumal, A.K. Ganguli, *Bull. Mater. Sci.* **25**, 259 (2002).
13. Jae Ho Yang, Woong Kil Choo, Jin Ho Lee, Chang Hee Lee, *Acta Cryst. B* **55**, 348 (1999).
14. A.A. Bush, V.P. Sirotinkin, *Inorg. Mater.* **44**, 1233 (2008).
15. Shashank Priya, Cheol-Woo Ahn, Sahn Nahm, *Ferroelectrics* **322**, 75 (2005).
16. A.A. Ostroushko, *Inorg. Mater.* **40**, 195 (2004).
17. K. Sambasiva Rao, P.S. Jagga Rao, K. Rama Rao, A.V. Prasada Rao, A.I. Robin, R.P. Tandon, *Ferroelectrics Lett.* **16**, 195 (1993).
18. Bhagwati Bishnoi, P.K. Mehta, Ravi Kumar, *Proc. of the 53rd DAE Solid State Physics Symposium* (2008).
19. Bhagwati Bishnoi, P.K. Mehta, Ravi Kumar, R.J. Choudhary, D.M. Phase, *Integrated Ferroelectrics* **119**, 1 (2010).
20. Jiang Yin, Zhigang Zou, Jinhua Ye, *J. Phys. Chem. B* **107**, 4936 (2003).
21. V. Ting, Y. Liu, L. Nore´n, R.L. Withers, D.J. Goossens, M. James, C. Ferraris, *J. Solid State Chem.* **177**, 4428 (2004).
22. V. Ting, Y. Liu, R.L. Withers, *Physica B* **385-386**, 558 (2006).
23. K. Jonscher, *Nature* **267**, 673 (1977).
24. B.K. Singh, B. Kumar, *Crystal Res. Technol.* **45**, 1003 (2010).
25. J. Maier, *Solid State Ionics*, *Part II. Aspects of nanoionics* **157**, 327 (2003).
26. D.C. Sinclair, A.R. West, *J. Appl. Phys.* **66**, 3850 (1989).
27. D.C. Sinclair, A.R. West, *J. Mat. Sci.* **29**, 6061 (1994).
28. V. Gupta, A. Mansingh, *Phys. Rev. B* **49**, 1989 (1994).
29. S. Dutta, A. Mansingh, *Phys. Rev. B* **49**, 1989 (1994).
30. Dillip K. Pradhan, B.K. Samantaray, R.N.P. Choudhary, Awalendra K. Thakur, *Mater. Sci. Eng. B* **116**, 7 (2005).
31. J.R. Macdonald (Ed.), *Chapter 4* (Wiley: Singapore: 1987).
32. V.V. Kharton, F.M.B. Marques, *Curr. Opin. Solid State Mater. Sci.* **6**, 261 (2002).
33. S.J. Hong, K. Meheta, A.V. Virkar, *J. Electrochem. Soc.* **145**, 638 (1998).
34. B.C.H. Steele, *Solid State Ionics* **129**, 95 (2000).
35. G.M. Christie, F.P.F. Van Berkle, *Solid State Ionics* **83**, 17 (1996).
36. Uraiwan Intatha, Sukum Eitssayeam, John Wang, Tawee Tunkasiri, *Curr. Appl. Phys.* **10**, 21 (2010).
37. Y.J. Li, X.M. Chen, R.Z. Hou, Y.H. Tang, *Solid State Commun.* **137** 120 (2006).
38. F. Yakuphanoglu, *Physica B* **393**, 139 (2007).
39. A. Dutta, T.P. Sinha, P. Jena, S. Adak, *J. Non- Cryst Solids* **354**, 3952 (2008).
40. L.N. Patro, K. Hariharan, *Mater. Chem. Phys.* **116**, 81 (2009).
41. L.N. Patro, K. Hariharan, *Mater. Sci. Eng. B* **162**, 173, (2009).
42. J. Tauc, *phys. status solidi* **15**, 627 (1966).